

THE PHOTODISINTEGRATION OF RARE EARTH ELEMENTS

By H. H. THIES*† and B. M. SPICER*

[Manuscript received March 10, 1960]

Summary

The neutron yields from praseodymium, terbium, and holmium have been measured as a function of bremsstrahlung energy, and from these the shapes of the respective cross sections have been deduced. For terbium and holmium, the cross section for photon absorption shows two peaks, in agreement with the predictions of both the hydrodynamic model and the independent particle model of the nuclear photoeffect in non-spherical nuclei. The case of praseodymium was treated as a control experiment, since this nucleus is nearly spherical. Its photon absorption cross section has only one peak, in agreement with expectation for a spherical nucleus. The results are discussed in terms of both the hydrodynamic model and the independent particle model. Values of the deformation parameter are deduced from the photodisintegration data and are compared with values obtained by other methods.

I. INTRODUCTION

Both collective theory (Danos 1956, 1958 ; Okamoto 1956, 1958) and shell model theory (Wilkinson 1956, 1958) predict that in non-spherical heavy nuclei the photonuclear giant resonance is broadened and will show two maxima if the nuclear deformation is large enough. Known nuclear electric quadrupole moments indicate that the nuclear deformation increases from a negligible amount for elements of atomic mass near 140 to a maximum for A near 170, and decreases again to small values for A near 200. Thus, by systematically investigating the shape of the giant resonance for nuclei over this mass range, it should be possible to demonstrate experimentally any broadening and splitting effect in the giant resonance. This would then lead to the testing of theories on the subject, and possibly to the use of photodisintegration data for the evaluation of nuclear deformations and electric quadrupole moments.

In the heavy elements it is not practicable to observe the photonuclear absorption cross sections directly. However, to a fair degree of approximation, they can be derived from photoneutron cross sections for these elements. The approximation here arises because of the need to correct for multiple neutron emission. Because of the very high Coulomb barrier, the emission of charged particles gives negligible contribution.

If the photoneutrons are to be observed directly, only mono-isotopic or almost mono-isotopic elements may be used as targets if separated isotopes are not available. In the region of interest here these are all odd-mass nuclei, namely : ^{139}La , ^{141}Pr , ^{159}Tb , ^{165}Ho , ^{169}Tm , ^{175}Lu , ^{181}Ta , ^{197}Au , ^{209}Bi .

* Physics Department, University of Melbourne.

† Present address : Physics Department, University of Western Australia, Nedlands, W.A.

In a previous paper (Spicer *et al.* 1958) an experiment on the photonuclear giant resonance in ^{139}La and ^{181}Ta was reported. This experiment used direct neutron detection (BF_3 -counters in a paraffin moderator). Simultaneously a similar very accurate experiment on ^{159}Tb , ^{181}Ta , ^{197}Au was performed independently by Fuller and Weiss (1958). In the present paper further direct neutron detection experiments on ^{141}Pr , ^{159}Tb , and ^{165}Ho are reported.

This type of experiment measures the total neutron production cross section

$$\sigma_{\gamma, \Sigma n} = \sigma_{\gamma, n} + 2\sigma_{\gamma, 2n} + 3\sigma_{\gamma, 3n} + \dots$$

The computation of the absorption cross section from $\sigma_{\gamma, \Sigma n}$ above the $(\gamma, 2n)$ threshold requires a knowledge of the ratio $S = \sigma_{\gamma, n} / \sigma_{\gamma, 2n}$. S may be estimated from statistical theory of nuclear reactions (Blatt and Weisskopf 1952). For the nucleus ^{165}Ho it was possible to determine S experimentally by combining the results from the direct neutron detection experiment with those from an independent activation experiment on the reaction $^{165}\text{Ho}(\gamma, n)$.

The available experimental results on ^{139}La , ^{141}Pr , ^{159}Tb , ^{165}Ho , ^{181}Ta , and ^{197}Au will be discussed in the light of theoretical predictions.

II. THEORETICAL DESCRIPTION OF THE PHOTONUCLEAR EFFECT

The predictions of the hydrodynamic theory have been discussed previously (Spicer *et al.* 1958) and lead to the result that the two eigenvalues are related by the equation

$$E_b/E_a = \hbar\omega_b/\hbar\omega_a = 0.911a/b + 0.089.$$

Here a refers to the semi-axis of rotational symmetry and b to the semi-axis perpendicular to a . If $(E_b - E_a)$ is large enough, the positions of E_a and E_b will coincide approximately with the positions of the experimental maxima (E_1 and E_2). Frictional coupling between the two eigen-modes will tend to decrease $(E_2 - E_1)$ and flatten the minimum between E_1 and E_2 .

Wilkinson (1958) used the Nilsson level scheme and computed photonuclear absorption cross sections for $140 < A < 210$. His results show that cross sections in non-deformed nuclei have one narrow maximum. This is broadened in deformed nuclei, and for $A=165$ the computed cross section is split into two separated maxima.

Wave functions and transition probabilities corresponding to the Nilsson Hamiltonian can be computed (see Nilsson 1955). They do, however, depend much more sensitively on the form of the chosen Hamiltonian than do the transition energies, and thus the computation of transition probabilities is not significant for excitation energies in the region 10–25 MeV. It is possible, however, to predict semiquantitatively the manner in which the nuclear deformation will affect electric dipole absorption cross sections, without actually knowing the strength of the $E1$ transitions individually. In the spheroidal nucleus, nuclear states are specified by different quantum numbers than in the spherical case. Thus, new selection rules (Alaga 1955, 1957) become increasingly effective with increasing nuclear deformation. In deformed nuclei, these selection rules separate the allowed electric dipole transitions into two groups. In transitions

of group I, the excitation energy is used predominantly to add energy to the component of motion of one nucleon in the direction of a , the axis of rotational symmetry. In group II, the energy is added predominantly to the component of motion in a direction perpendicular to a .

The systematic shift of levels with deformation of a prolate type causes excitation energies for group I transitions to be smaller than for group II transitions, in general. (For an oblate spheroid, the opposite condition tends to hold.) Also, as a consequence of the selection rules, there are approximately

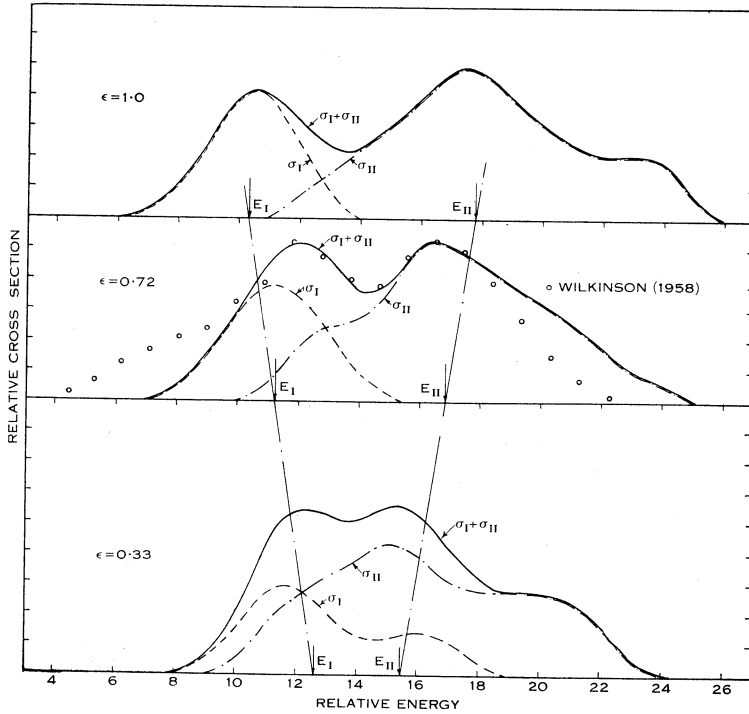


Fig. 1.—Cross section for photon absorption in ^{166}Ho computed from the Nilsson level scheme. The three cross sections are for different assumed nuclear deformations.

twice as many allowed $E1$ transitions in group II as in group I. Thus the $E1$ absorption cross section will separate into two giant resonance components. These components will have mean energies of E_I and E_{II} respectively. This does not mean that the maxima in the composite cross section will occur at E_I and E_{II} (see Fig. 1). For deformations insufficient to give rise to separation of the peaks, a single broadened peak will result.

For particular nuclei, we investigated the broadening and splitting effect in the following manner. From the Nilsson level diagram (Nilsson 1955) the excitation energies of the electric dipole transitions allowed by the selection rules are found. In the first approximation, it is assumed that all the allowed transitions have equal strength. The corresponding absorption lines are given

half-width Γ_{level} , and a Gaussian shape. Contributions from the various transitions are summed at a series of intervals. The value of Γ_{level} may be taken as 3 MeV, since this is an estimated value for non-deformed nuclei given by Wilkinson (1956). However, it is possible that this value may be less than 3 MeV for strongly deformed nuclei, as in this case the level degeneracies are reduced considerably. Component $E1$ cross sections σ_{I} and σ_{II} , corresponding to transitions in groups I and II, may be derived separately. Although the strengths of transitions may vary considerably from equality, these variations will not affect the shape and position of σ_{I} and σ_{II} significantly, as in this region of A the number of transitions is large. For example, for A near 160, there are 14 proton transitions in group I and 28 in group II. The cross sections σ_{I} and σ_{II} , and their sum σ_{abs} , for the nucleus ^{165}Ho are shown on Figure 1. The calculations were made for three values of the deformation.

It was found empirically from a number of diagrams similar to Figure 1 that the positions of E_{I} and E_{II} , the mean energies of σ_{I} and σ_{II} , follow the relationship

$$E_{\text{II}}/E_{\text{I}} = 1 + 0.7\varepsilon. \quad \dots\dots\dots (1)$$

Here ε is the deformation parameter (Danos 1958) defined by

$$\varepsilon = (a^2 - b^2)/R^2. \quad \dots\dots\dots (2)$$

It is related to the deformation parameter δ of Nilsson (1955) by the relationship

$$\varepsilon = 2\delta(1 + 0.66\delta). \quad \dots\dots\dots (3)$$

R is the radius of a sphere having the same volume as the spheroid. ($R^3 = ab^2 = r_0^3 A$. Throughout this paper, the value $r_0 = 1.2$ fermi is used (Ford and Hill 1955).) Thus the independent particle model predicts that the giant resonance is broadened in non-spherical nuclei, and, for large deformations, splits into two maxima in a manner similar to that predicted by the hydrodynamic model.

Using equation (2), the prediction of the hydrodynamic theory may be expressed in terms of an expansion in ε as follows

$$E_b/E_a = 1 + 0.46\varepsilon + \text{terms of order } (\varepsilon^2). \quad \dots\dots\dots (4)$$

In view of the crudeness of the assumptions which led to (1) and (4), the predictions on the splitting effect from hydrodynamic theory and from independent particle model theory are in substantial agreement. This is so in spite of the very different assumptions in the two theories.

III. EXPERIMENTS ON PHOTONEUTRONS FROM

^{141}Pr , ^{159}Tb , AND ^{165}Ho

Bremsstrahlung from the Melbourne 18 MeV electron synchrotron was used to irradiate the targets. Each target consisted of 10 g of a rare earth oxide in powder form (Pr_6O_{11} , Tb_4O_7 , Ho_2O_3). The oxide was contained as a tablet in a polystyrene container. Sample impurities consisted of neighbouring rare earths, and were smaller than 1 per cent. in each case. The absorption of γ -rays in the target and the container lid was less than 3 per cent. in all cases, and was taken into account in the yield analysis.

With the exception of an activation experiment on the reaction $^{165}\text{Ho}(\gamma, n)$, the photoneutrons were detected by BF_3 -counters embedded in a paraffin moderator. The arrangement of target, BF_3 -counters, paraffin moderator, and concrete "house" was essentially the same as that described by Spicer *et al.* (1958). Four BF_3 -counters, separated from the target by 12.5 cm of paraffin, were grouped as two pairs, and the counts from these were recorded through two independent electronic counting systems. The electronic counting loss in each system was determined experimentally and was kept less than 1.2 per cent. by limiting the yield rate of the synchrotron when necessary. Corrections were made for the counting loss. The neutron detection efficiency of each counting system was checked before and after each run by inserting a Ra-Be neutron source into an accurately reproducible position in the paraffin moderator and recording the counts obtained per minute. The number of neutrons counted in a given run was thereby corrected for the average deviation in neutron detection efficiency from a standard average value.

The γ -ray dose was measured by using a 25 r Victoreen thimble as a transmission ionization chamber. The leakage of this instrument was measured periodically and found to be negligible over several days. Each run was arranged so as to make the recorded dose approximately 10 r, thus effectively eliminating any relative error that would arise from a calibration error in the Victoreen scale. Temperature and pressure were recorded before and after each run and a temperature-pressure correction was applied to each dose reading.

The energy scale of the synchrotron had been calibrated previously by means of photoneutron threshold measurements (Spicer *et al.* 1958). This calibration was checked periodically by measuring the $^{55}\text{Mn}(\gamma, n)$ threshold.

For proper interpretation of the experimental results, the standard error in each yield point must be known. This error may be substantially greater than the purely statistical counting error. It can be estimated only inadequately from the reproducibility of neutron counts, γ -ray dose measurements, and energy settings of the accelerator, but can be obtained accurately if a yield ordinate has been measured many times at random time intervals during a complete experiment.

During each experiment, individual yield ordinates were measured in some instances up to 14 times, and it was found that the spread of values obtained at each energy setting followed a normal distribution within statistical accuracy. Experiments were performed with praseodymium, terbium, and holmium targets in position and background runs were made with the empty containers in the target position. The background remained unaltered when the empty polystyrene container was removed.

The contribution of photoneutrons from the oxygen content of the rare earth oxide samples was estimated. Under all circumstances its contribution to the total neutron production was less than 1 per cent.

Yield ordinates were measured at 0.25 MeV intervals from 7 to 18 MeV. These results are shown in Figures 2, 3, 4, for praseodymium, terbium, and holmium respectively. Smooth yield curves were drawn through each discrete set of ordinates, fitting by eye with minimum curvature curves. For the

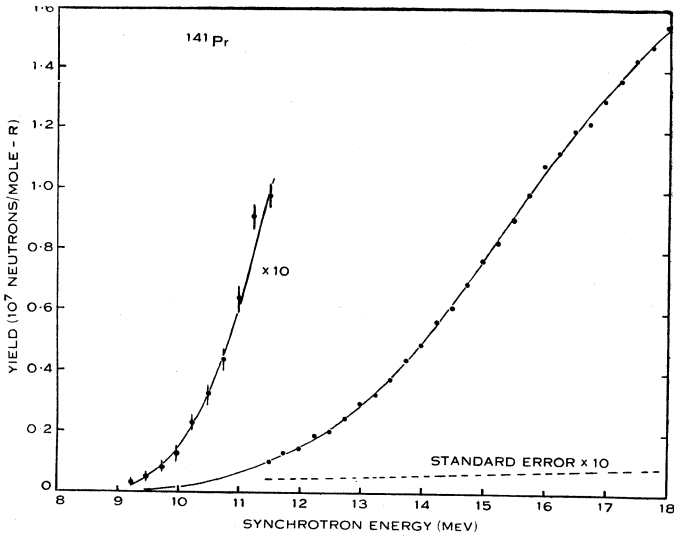


Fig. 2.—Total neutron yield from praseodymium.

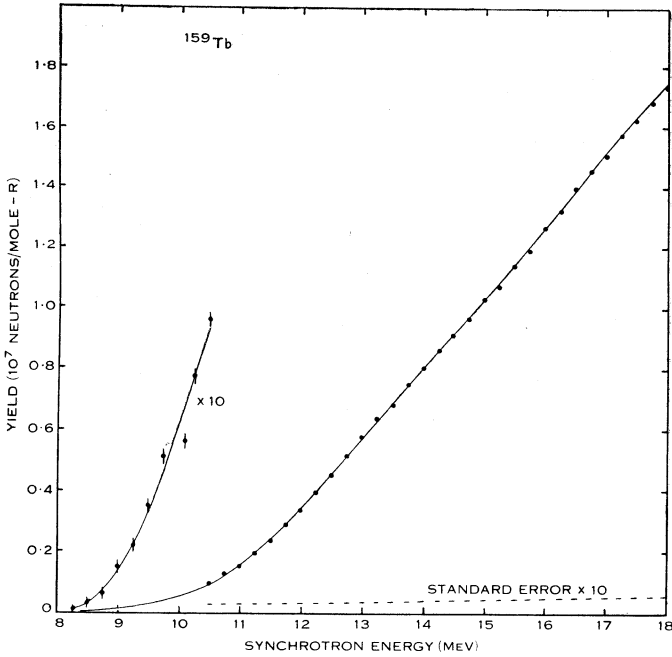


Fig. 3.—Total neutron yield from terbium.

transformation of yield data to cross sections for photoneutron production the tables of Penfold and Leiss (1958), having $\Delta E=1$ MeV, were used. Each set of measured yield ordinates was separated into four subsets, each subset having $\Delta E=1$ MeV. These subsets were then analysed separately, and the resultant cross sections were then combined to make a composite cross section. Thus, the cross section ordinates making up one "unsmoothed" cross section curve come from four interlaced and independent sets of "unsmoothed" cross section ordinates. Standard errors of unsmoothed cross section values were computed from standard errors of yield ordinates.

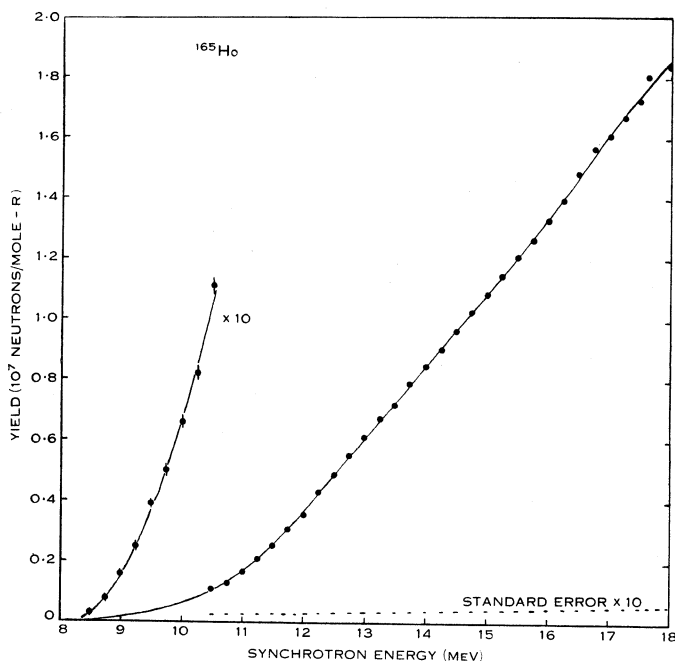


Fig. 4.—Total neutron yield from holmium.

The smooth cross sections shown were obtained from analysis of the smoothed yield curves as drawn through the experimental points. Values of the yield were read off this smooth curve and these were treated in the same manner as the unsmoothed yield points. The cross sections are shown in Figures 5 (¹⁴¹Pr), 6 (¹⁵⁹Tb), and 7 (¹⁶⁵Ho). The results on terbium and holmium are the averages from two independent experiments. These results agreed within the standard errors and demonstrated the reproducibility of results. Note that these cross sections are the total neutron production cross sections.

To reconstruct the photon absorption cross section $\sigma_{\text{abs}} = \sigma_{\gamma,n} + \sigma_{\gamma,2n}$ from the total neutron production cross section $\sigma_{\gamma,\Sigma n} = \sigma_{\gamma,n} + 2\sigma_{\gamma,2n}$, allowance has to be made for neutron multiplicity above the $(\gamma,2n)$ threshold.

(γ,n) thresholds of some rare earths have recently been measured by Geller, Muirhead, and Halpern (Muirhead, personal communication 1959), and agree

within less than 0.3 MeV with those calculated from the semi-empirical mass formula of Cameron (1957). Therefore this formula was used to calculate the values of $(\gamma, 2n)$ thresholds. The values obtained were 17.6 MeV for $^{141}\text{Pr}(\gamma, 2n)$,

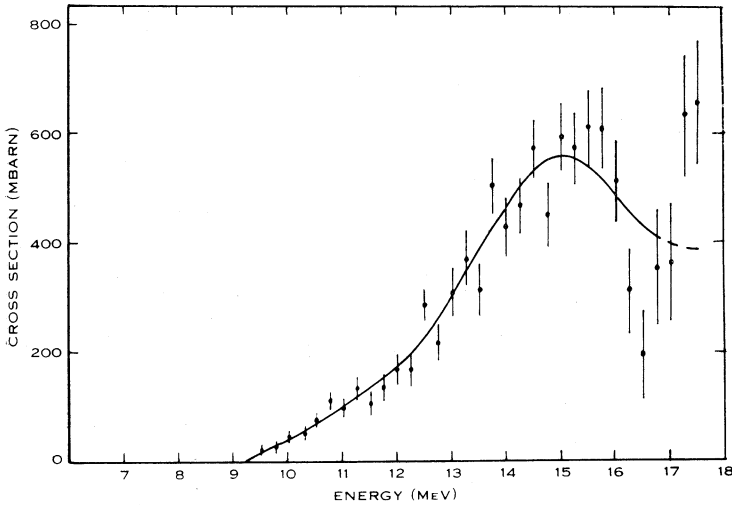


Fig. 5.—Total neutron production cross section for ^{141}Pr . The points are obtained by analysis using the experimental points. The smooth curve is obtained by analysis of a smooth yield curve drawn through the experimental points.

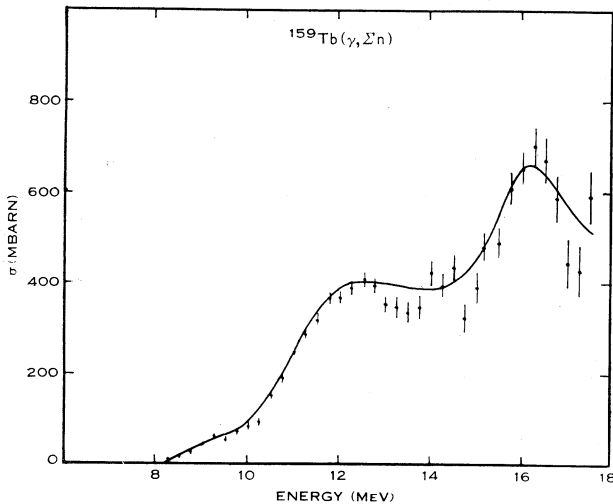


Fig. 6.—Total neutron production cross section for ^{159}Tb .

14.8 MeV for $^{159}\text{Tb}(\gamma, 2n)$, and 14.4 MeV for $^{165}\text{Ho}(\gamma, 2n)$. Thus, in the present experiment on ^{141}Pr , the neutron multiplicity need not be considered.

Blatt and Weisskopf estimated the neutron multiplicity using statistical theory of nuclear reactions. Applied to the present instance, this does not take

account of the neutrons emitted in a direct photoeffect. This can be built in to the statistical theory estimate, which then becomes

$$\sigma_{\gamma,n} + \sigma_{\gamma,2n} = \frac{\sigma_{\gamma,n} + 2\sigma_{\gamma,2n}}{1 + (1-x)\{1 - (1+k/\Theta)e^{-k/\Theta}\}} \dots\dots\dots (5)$$

Here x is the fraction of direct events to total number of events, k is the energy difference between the incident photon energy and the $(\gamma,2n)$ threshold value,

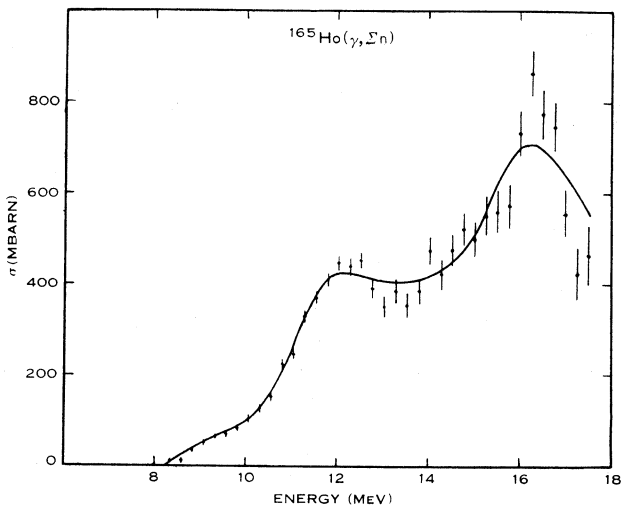


Fig. 7.—Total neutron production cross section for ^{165}Ho .

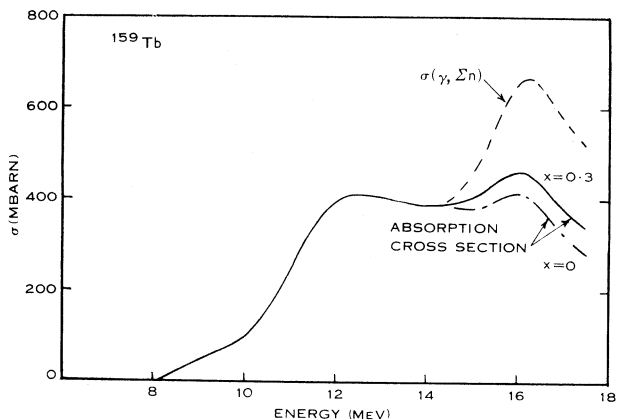


Fig. 8.—Cross section for photon absorption in ^{159}Tb , using statistical theory of nuclear reactions to correct for neutron multiplicity. The factor x is a measure of the probability that a direct photoeffect will occur.

and Θ MeV is the nuclear temperature of the target nucleus less one neutron. Values of Θ were obtained from Blatt and Weisskopf (1952).

Equation (5) can be brought into agreement with measured data on neutron multiplicities if a value of x between 0.3 and 0.4 is assumed. Experimental

data considered are by Montalbetti, Katz, and Goldemberg (1953), Whalin and Hanson (1953), Berman and Brown (1954), Silva, Goldemberg, and Smith (1958), and Carver and Turchinets (1959*a*, 1959*b*).

The cross sections in ^{159}Tb and ^{165}Ho , corrected for neutron multiplicity, are shown in Figures 8 and 9. Curves are drawn for values of x of zero and 0.3.

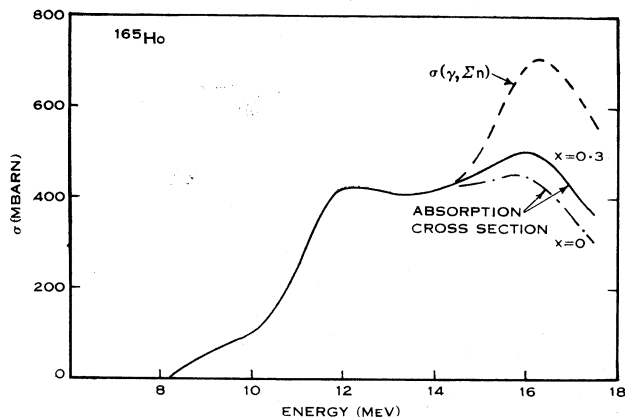


Fig. 9.—Cross section for photon absorption in ^{165}Ho . The correction for neutron multiplicity is applied using statistical theory.

IV. ACTIVATION EXPERIMENT

The (γ, n) cross section in ^{165}Ho was determined from a separate experiment by counting the β -activity of the daughter nucleus ^{164}Ho . Brown and Becker (1954) give the half-life of this nuclide as 36.7 min. The β -spectrum has a maximum energy of 0.99 MeV.

The Ho_2O_3 used in the BF_3 -counter experiment was subdivided into nine samples of 1.050 g each. These were each pressed into tablet form (1.4 cm diameter by 0.18 cm) in identical polystyrene containers, and protected by 0.32 cm thick "Perspex" lids. The containers could be located accurately and reproducibly in a jig 30 cm from the synchrotron target. Dose measurements were made in the manner previously described. In this experiment the γ -ray beam traversed the target before striking the Victoreen thimble. The absorption of γ -rays in the target was therefore allowed for in the analysis.

The container lid was removed for counting the activity. This was commenced 5 min after the cessation of irradiation (to allow the ^{15}O 2-min activity to die out to some extent) and continued for 30 min. Only pure 37-min activity of ^{164}Ho could be detected. Allowance was made for the finite dead-time of the Geiger counting system, and the appropriate correction applied to the results.

A procedure was developed to allow for the decay of the activity during irradiation, and for variations in the yield rate of the synchrotron. The γ -ray beam, after traversing the dosimeter, was allowed to strike a 500 g lead sample. This was located in the "sample position" in the paraffin moderator plus BF_3 -counter assembly that had been used for the direct neutron detection experiments. The counters therefore received copious photoneutrons from the

lead sample. The number of neutrons recorded in any time interval is proportional to the γ -ray dose given in that time. The neutron counts were recorded at 2-min intervals and used as a relative measure of the dose which the holmium sample had received during that interval. The decay of the activity of the holmium sample during the 30 min irradiation period could then be calculated with due allowance for variations in dose rate.

Activation points were taken at four energies below the $(\gamma,2n)$ threshold, and at 0.25 MeV intervals above 14.5 MeV. Each point was repeated at least twice. A smooth curve was fitted to the measured points (see Fig. 10). This curve was normalized to the total neutron yield curve at the energies below the

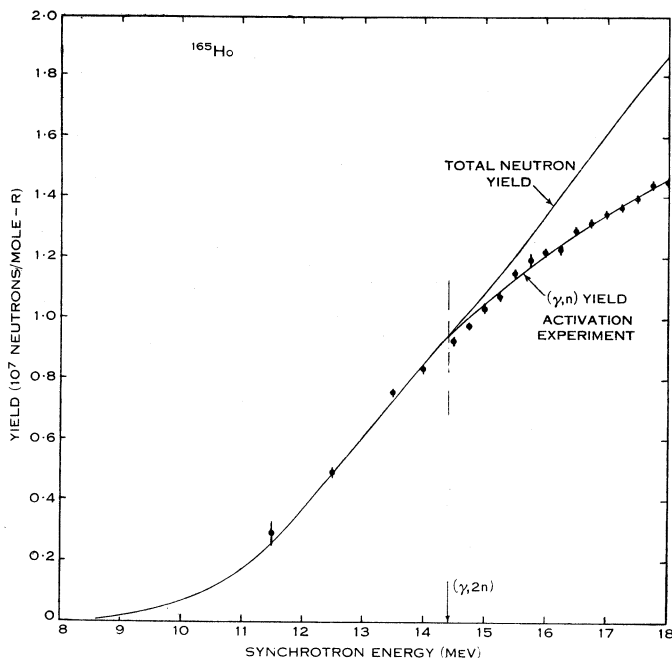


Fig. 10.—Yield curve for the $^{165}\text{Ho}(\gamma,n)^{164}\text{Ho}$ reaction, measured by counting the ^{164}Ho activity. It was normalized on to the total neutron yield curve for holmium below the $(\gamma,2n)$ threshold.

$(\gamma,2n)$ threshold at which the activity was measured. The (γ,n) cross section at energies above the $(\gamma,2n)$ threshold was computed from the yield curve in the manner previously described, and is shown as $\sigma_{\gamma,n}$ on Figure 11. On the same figure the total neutron cross section $\sigma_{\gamma,\Sigma n}$ is shown. It is to be noted that the yield curve for the ^{164}Ho activity has not been measured well enough for analysis using the experimental points to be useful. Consequently, all discussion of this cross section refers to the result of analysis of the smooth yield curve.

Using the total neutron cross section $\sigma_{\gamma,\Sigma n}$ given by the BF_3 -counter experiment and the (γ,n) cross section of the activation experiment, the photon absorption cross section is given by

$$\sigma_{\text{abs}} = \sigma_{\gamma,n} + \sigma_{\gamma,2n} = \frac{1}{2} \{ \sigma_{\gamma,\Sigma n} + \sigma_{\gamma,n} \}. \quad \dots \dots \dots (6)$$

The absorption cross section σ_{abs} computed with equation (6) is compared in Figure 12 with the absorption cross section computed using neutron multiplicity theory, using equation (5) with $x=0.3$. The two cross sections are in agreement within statistical expectations, although a value of x as high as 0.4 would be equally suitable.

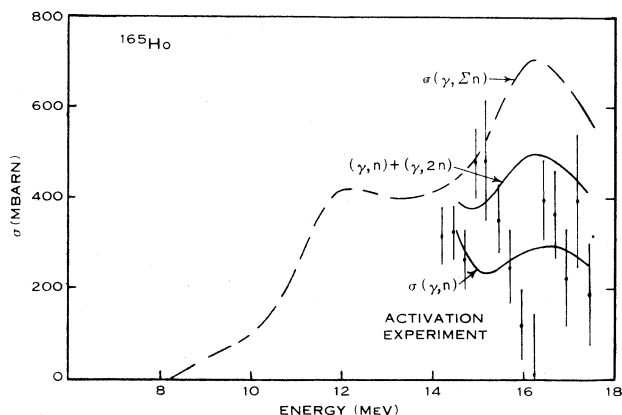


Fig. 11.—Result of analysis of the holmium activation experiment. Also plotted are the total neutron production cross section and the photon absorption cross section derived using the activation results.

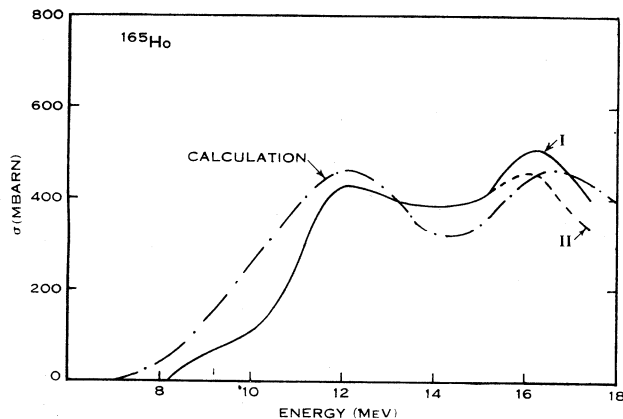


Fig. 12.—Comparison of the calculated cross section for photon absorption in ^{165}Ho with experimental measurements of the same quantity. Curve I has the neutron multiplicity correction applied using the activation experiment. Curve II has neutron multiplicity correction applied using statistical theory of nuclear reactions, with an assumed 30 per cent. direct photoeffect.

V. RESULTS

The derived γ -absorption cross section for the undeformed nucleus ^{141}Pr showed one narrow giant resonance maximum, whereas in the strongly deformed nuclei ^{159}Tb and ^{165}Ho the predicted broadening and splitting effect was observed. These results are consistent with those obtained for the spherical nuclei ^{139}La and ^{197}Au , and the deformed ^{159}Tb and ^{181}Ta , by Fuller and Weiss (1958) and

Spicer *et al.* (1958). In both sets of experiments essentially the same experimental technique was used.

When comparing the experimental results on photonuclear absorption cross sections with theoretical predictions, the notation given below will be used. The component of the giant resonance will have maximum cross section $(\sigma)_{\max}$ at energy E . The width of the resonance will be discussed in terms of $\Gamma_{-\frac{1}{2}}$ and $\Gamma_{+\frac{1}{2}}$, which give the energy difference between E and the energy at which the cross section is half its maximum value below and above the energy E respectively. The total width of the resonance, Γ , is given by $(\Gamma_{-\frac{1}{2}} + \Gamma_{+\frac{1}{2}})$. The integrated cross section I is in good approximation proportional to the product of $(\sigma)_{\max}$ and Γ . Thus the ratio of the integrated cross sections under two component peaks of a split giant resonance is given by

$$\frac{I_2}{I_1} = \frac{(\sigma_2)_{\max} \Gamma_2}{(\sigma_1)_{\max} \Gamma_1} = \frac{(\sigma_2)_{\max} \Gamma_{2,+\frac{1}{2}}}{(\sigma_1)_{\max} \Gamma_{1,-\frac{1}{2}}} \dots\dots\dots (7)$$

The total width of a double-peaked giant resonance shall be defined by

$$\Gamma_{G.R.} = \Gamma_{1,-\frac{1}{2}} + \Gamma_{2,+\frac{1}{2}} + E_2 - E_1 \dots\dots\dots (8)$$

The giant resonance parameters for ^{139}La , ^{141}Pr , ^{197}Au , ^{159}Tb , ^{165}Ho , and ^{181}Ta are collected in Tables 1 and 2.

TABLE 1
GIANT RESONANCE PARAMETERS FOR NON-DEFORMED NUCLEI

Nucleus.. ..	^{139}La	^{141}Pr	^{197}Au
Reference ..	Spicer <i>et al.</i> (1958)	Present Paper	Fuller and Weiss (1958)
E (MeV)	14.9	15.1	13.5
$(\sigma)_{\max}$ (mbarn)	460	480	590
$2 \times \Gamma_{-\frac{1}{2}}$ (MeV)	4.2	4.4	4
$\Gamma_{G.R.}$ (MeV)	4.2	—	4.2

TABLE 2
GIANT RESONANCE PARAMETERS IN DEFORMED NUCLEI

Nucleus ..	^{159}Tb		^{165}Ho	^{181}Ta	
	Fuller and Weiss (1958)	Present Paper	Present Paper	Fuller and Weiss (1958)	Spicer <i>et al.</i> (1958)
$\Gamma_{G.R.}$ (MeV)	6.5	6.7 ± 0.5	7 ± 0.5	6.2 ± 0.2	6.1
E_1 (MeV)	12.5	12.4 ± 0.2	12.1 ± 0.2	12.45	12.6
$(\sigma_1)_{\max}$ (mbarn)	260	410	420	308	500
Γ_1 (MeV)	2.4	3.3	2.8	2.3	2.0
E_2 (MeV)	16.3	16.0 ± 0.2	16.2 ± 0.2	15.45	15.3
$(\sigma_2)_{\max}$ (mbarn)	310	460	510	348	450
Γ_2 (MeV)	4.0	4.5	4.7	4.4	4.0
I_2/I_1 ..	2.0	2.0	2.0	2.16	1.8
E_2/E_1 ..	1.30	1.29 ± 0.03	1.34 ± 0.03	1.25 ± 0.01	1.21 ± 0.03

VI. INTERPRETATION OF RESULTS

If the experimentally determined values of E_1 and E_2 are equated to the E_a and E_b respectively of the Danos-Okamoto theory, the nuclear deformation parameter may be calculated from equation (4) by inserting the relevant values from Table 2. These values are entered in Table 3.

The independent particle model theory may also be used to obtain values of the nuclear deformation. The shapes of the cross sections were calculated from the energy level diagram of Nilsson (1955), and the value of ϵ was estimated by comparing the computed cross sections with the experimental ones. The comparison for the case of ^{165}Ho is shown in Figure 12.

TABLE 3
NUCLEAR QUADRUPOLE MOMENTS AND DEFORMATION IN ^{159}Tb , ^{165}Ho , AND ^{181}Ta

Method	Nucleus	ϵ	Q_0 (barn)	Reference
Coulomb excitation ..	^{159}Tb	0.69	8.1	Martin, Marmier, and de Boer (1958)
Coulomb excitation ..		0.63	6.9	Alder <i>et al.</i> (1956)
Survey, low-lying levels ..		0.74	—	Mottelson and Nilsson (1959)
Photodisintegration (Danos)		0.63	7.0 ± 0.7	Present paper
Photodisintegration (IPM)		0.72	8.0 ± 0.8	Present paper
Paramagnetic resonance ..	^{165}Ho	0.4	+4.3	Baker and Bleaney (1955)
Coulomb excitation ..		0.69	8.0	Martin, Marmier, and de Boer (1958)
Coulomb excitation ..		0.67	7.8	Alder <i>et al.</i> (1956)
Survey, low-lying levels ..		0.72	—	Mottelson and Nilsson (1959)
Photodisintegration (Danos)		0.74	8.6 ± 0.9	Present paper
Photodisintegration (IPM)		0.72	8.4 ± 0.9	Present paper
Atomic spectroscopy ..	^{181}Ta	0.43	$+5.8 \pm 0.5$	Murakawa and Kamei (1957)
Coulomb excitation ..		0.41	5.6	Martin, Marmier, and de Boer (1958)
Coulomb excitation ..		0.50	6.8	Alder <i>et al.</i> (1956)
Survey, low-lying levels ..		0.53	—	Mottelson and Nilsson (1959)
Photodisintegration (Danos)		0.54	7.0	Fuller and Weiss (1958)
Photodisintegration ..		0.46	6.0	Spicer <i>et al.</i> (1958)

If the nuclear charge is assumed to be uniformly distributed throughout the nucleus, the values of ϵ obtained may be used to compute a value of Q_0 , the intrinsic nuclear electric quadrupole moment. The quadrupole moment of a charge Ze uniformly distributed throughout a spheroid is given by

$$Q_0 = 0.4Z(a^2 - b^2). \dots\dots\dots (9)$$

The relation between ϵ and Q_0 is

$$\epsilon = 2.5Q_0/r_0^2ZA^\ddagger, \dots\dots\dots (10)$$

using equation (2) and $R^3 = r_0^3A$. In Table 3 the values of ϵ and Q_0 obtained from the photodisintegration data are set out. Also shown in Table 3 are values

for ε and Q_0 obtained from measurements of atomic spectra, from Coulomb excitation measurements, and from a survey of the low-lying levels of deformed nuclei.

The theory of fast electric quadrupole transitions between low-lying levels (Coulomb excitation) and of the spacings of low-lying levels in deformed nuclei are based on the collective theory of nuclear rotational states (Bohr and Mottelson 1953). Both of these types of study give values of Q_0^2 directly in terms of the collective theory, and therefore do not specify the sign of Q_0 . The accuracy of such Q -values is limited to some 20 per cent. still, due to the inherent difficulties in the absolute measurements necessary. To compute the deformation parameter ε , again some sort of assumption has to be made concerning the nuclear charge distribution. Again, we assume a uniform charge distribution.

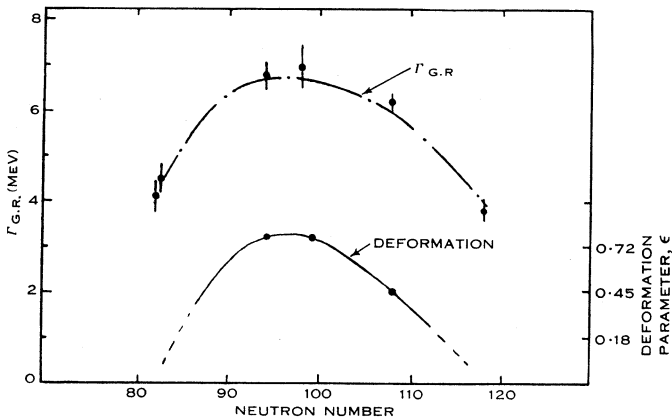


Fig. 13.—Plot of $\Gamma_{G.R.}$ and ε as a function of neutron number over the region of interest.

The atomic spectroscopy measurements do not give the value of Q_0 immediately. Rather they give a value of the quadrupole moment with respect to the nuclear angular momentum direction, say Q , which is less than the value of Q_0 . Q_0 is the quadrupole moment relative to the direction of the nuclear axis of symmetry, which in strongly deformed nuclei is not necessarily in the same direction as the angular momentum vector. In the extreme case of strong coupling (Bohr and Mottelson 1953) Q and Q_0 are related by $Q = Q_0 P_I$, where

$$P_I = \frac{I(2I-1)}{(I+1)(2I+3)}$$

and I is the ground state spin. Okamoto (1958) has argued for the validity of the strong coupling approximation in the case of the nuclei ^{159}Tb , ^{165}Ho , ^{181}Ta .

It must be pointed out that the comparison of the above data with photodisintegration data should be treated with some caution. The three alternative methods of determining nuclear deformations which were mentioned are all concerned with nuclei in their ground state or in states very near it. In contrast, photodisintegration data concern transitions between the ground state and

excited states 15–20 MeV above the ground state. Again, Okamoto (1958) has argued that the comparison made here is worth while, and the close agreement exhibited in Table 3 indicates that his argument may be correct.

It is to be noted that the ratios I_2/I_1 noted in Table 2 do approximately fulfil the theoretical prediction of the value 2 for that ratio.

On Figure 13 the values of ϵ and of $\Gamma_{G.R.}$ are plotted as a function of the neutron number N . It is seen that the broadening effect in the photonuclear giant resonance is dependent on nuclear deformation.

VII. CONCLUSION

The quantitative investigation of the broadening and splitting effect in the photonuclear giant resonance, in particular the latter effect, requires extremely accurate experiments. The splitting effect remained unobserved in earlier experiments because in those cases the experimental resolution was not sufficient.

The splitting effect was not observed in the (γ, n) cross sections of ^{139}La , ^{141}Pr , and ^{197}Au . This is in agreement with the prediction that the effect will not be present for non-deformed nuclei. This does not exclude the possibility of some fine structure in these cross sections, but merely states that the experimental resolution at present attainable is insufficient to detect it.

The experimental resolution in the experiments of Fuller and Weiss (1958), Spicer *et al.* (1958), and of the present work was sufficient to indicate that the splitting effect observed is real. A discussion of the resolution of bremsstrahlung experiments is given by Thies (to be published). The predictions on photonuclear absorption cross sections from hydrodynamic theory and from independent particle model theory are very much alike, and are in excellent agreement with observation. It was not possible to decide whether experimental cross sections favour either one of the two theories.

VIII. ACKNOWLEDGMENT

One of the authors (H.H.T.) held an I.C.I.A.N.Z. research fellowship during most of this work.

IX. REFERENCES

- ALAGA, G. (1955).—*Phys. Rev.* **100**: 432.
 ALAGA, G. (1957).—*Nuclear Phys.* **4**: 625.
 ALDER, K., BOHR, A., HUUS, T., MOTTELSON, B. R., and WINTHER, A. (1956).—*Rev. Mod. Phys.* **28**: 432.
 BAKER, J. M., and BLEANEY, B. (1955).—*Proc. Phys. Soc. A* **68**: 1090.
 BERMAN, A. I., and BROWN, K. L. (1954).—*Phys. Rev.* **96**: 83.
 BLATT, J. M., and WEISSKOPF, V. F. (1952).—“Theoretical Nuclear Physics.” p. 379. (Wiley: New York.)
 BOHR, A., and MOTTELSON, B. R. (1953).—*Math-fys. Medd.* **27**, No. 16.
 BROWN, H. N., and BECKER, R. A. (1954).—*Phys. Rev.* **96**: 1372.
 CAMERON, A. G. W. (1957).—Atomic Energy of Canada Ltd. Report CRP 690.
 CARVER, J. H., and TURCHINETZ, W. (1959a).—*Proc. Phys. Soc.* **73**: 69.
 CARVER, J. H., and TURCHINETZ, W. (1959b).—*Proc. Phys. Soc.* **73**: 110.
 DANOS, M. (1956).—*Bull. Amer. Phys. Soc.* **1**: 135, 246.
 DANOS, M. (1958).—*Nuclear Phys.* **5**: 23.
 FORD, K. W., and HILL, D. L. (1955).—*Annu. Rev. Nuclear Sci.* **5**: 25.

- FULLER, E. G., and WEISS, M. S. (1958).—*Phys. Rev.* **112**: 560.
- MARTIN, M., MARMIER, P., and DE BOER, J. (1958).—*Helv. Phys. Acta* **31**: 435.
- MONTALBETTI, R., KATZ, L., and GOLDEMBERG, J. (1953).—*Phys. Rev.* **91**: 659.
- MOTTELSON, B. R., and NILSSON, S. G. (1959).—*Math-fys. Medd.* **1**, No. 8.
- MURAKAWA, K., and KAMEI, T. (1957).—*Phys. Rev.* **105**: 671.
- NILSSON, S. G. (1955).—*Math-fys. Medd.* **29**, No. 16.
- OKAMOTO, K. (1956).—*Progr. Theor. Phys., Osaka* **15**: 75.
- OKAMOTO, K. (1958).—*Phys. Rev.* **110**: 143.
- PENFOLD, A. S., and LEISS, J. E. (1958).—"Analysis of Photo Cross Sections." (Physics Research Laboratory, University of Illinois: Champaign, Illinois.)
- SILVA, E., GOLDEMBERG, J., and SMITH, P. B. (1958).—*Nuovo Cim.* **1**: 18.
- SPICER, B. M., THIES, H. H., BAGLIN, J. E., and ALLUM, F. R. (1958).—*Aust. J. Phys.* **11**: 298.
- WHALIN, E. A., and HANSON, A. O. (1953).—*Phys. Rev.* **89**: 324.
- WILKINSON, D. H. (1956).—*Physica* **22**: 1039.
- WILKINSON, D. H. (1958).—*Phil. Mag.* **3**: 567.